International Journal of Radiation Oncology biology • physics

www.redjournal.org

Biology Contribution

Cognitive and Imaging Differences After Proton and Photon Whole Brain Irradiation in a Preclinical Model

Tien T. Tang, PhD,[*] Janice A. Zawaski, PhD,[*] Shelli Kesler, PhD,[†] Christine A. Beamish, PhD,[‡] Taeko Inoue, PhD,[*] Emma C. Perez, PhD,[*] Lawrence Bronk, PhD,[§] Falk Poenisch, PhD,[‖] Tina M. Briere, PhD,[‖] Omaima M. Sabek, PhD,[‡] David R. Grosshans, MD, PhD,[§] and M. Waleed Gaber, PhD[*,¶]

[*]Department of Pediatrics, Hematology-Oncology Section, Dan L. Duncan Cancer Center, Baylor College of Medicine, Houston, Texas; [†]School of Nursing and Department of Diagnostic Medicine, Dell School of Medicine, University of Texas at Austin, Austin, Texas; [‡]Department of Surgery, Houston Methodist Research Institute, Houston, Texas; [§]Departments of Radiation and Experimental Radiation Oncology, UT—MD Anderson Cancer Center, Houston, TX; [‖]Department of Radiation Physics, UT—MD Anderson Cancer Center, Houston, Texas; and [¶]Department of Molecular Physiology & Biophysics, Baylor College of Medicine, Houston, Texas

Received Jan 11, 2021; Accepted for publication Sep 1, 2021

Purpose: Compared with photon cranial radiation therapy (X-CRT), proton cranial radiation therapy (P-CRT) offers potential advantages in limiting radiation-induced sequalae in the treatment of pediatric brain tumors. This study aims to identify cognitive, functional magnetic resonance and positron emission tomography imaging markers and molecular differences between the radiation modalities.

Methods and Materials: Juvenile rats received a single faction of 10 Gy (relative biological effectiveness−weighted dose) delivered with 6 MV X-CRT or at the midspread out Bragg peak of a 100 MeV P-CRT beam. At 3, 6, and 12 months post-CRT, executive function was measured using 5-choice serial reaction time task. At ∼12 months post-CRT, animals were imaged with ^{18}F-Flurodeoxy-glucose positron emission tomography imaging followed by functional ex vivo magnetic resonance imaging and stained for markers of neuroinflammation.

Results: Irradiated animals had cognitive impairment with a higher number of omissions and lower incorrect and premature responses compared with sham ($P \leq .05$). The accuracy of the animals' X-CRT was less than that of sham ($P \leq .001$). No significant difference in rates of cognitive change were found between the radiation modalities. At 12 months post-CRT, glucose metabolism was significantly higher than sham in X-CRT ($P = .04$) but not P-CRT. Using diffusion tensor imaging, P-CRT

Corresponding author: M. Waleed Gaber, PhD; E-mail: gaber@bcm.edu

Tien T. Tang and Janice A. Zawaski contributed equally to this work and share first authorship.

This work was supported by a grant from the National Cancer Institute (1R01CA208535) (D.R.G.) and the Cancer Prevention Research Institute of Texas (RP130573CPRIT) (M.W.G.).

Disclosures: none.

Research data will be shared upon request to the corresponding author.

Supplementary material associated with this article can be found, in the online version, at doi:10.1016/j.ijrobp.2021.09.005.

Acknowledgments—The authors thank Texas Children's Hospital for use of the Small Animal Imaging Facility.

Int J Radiation Oncol Biol Phys, Vol. 112, No. 2, pp. 554−564, 2022

https://doi.org/10.1016/j.ijrobp.2021.09.005

brains were found to have higher white matter volume and fiber lengths compared with sham ($P < .03$). Only X-CRT animals had higher apparent diffusion coefficient values compared with sham ($P = .04$). P-CRT animals had more connectomic changes compared with X-CRT. Correlative analysis identified several imaging features with cognitive performance. Furthermore, microgliosis ($P < .05$), astrogliosis ($P < .01$), and myelin thinning ($P < .05$) were observed in both radiation modalities, with X-CRT showing slightly more inflammation.

Conclusions: Both P-CRT and X-CRT lead to neurocognitive changes compared with sham. Although no significant difference was observed in neuroinflammation between the irradiated groups, differences were found in late-term glucose metabolism and brain connectome. Our results indicate that despite relative biological effectiveness weighting of the proton dose there are still differential effects which warrants further investigation.

Introduction

Medulloblastoma is the most common malignant brain tumor in children. The standard of care for patients with medulloblastoma includes surgical resection followed by craniospinal radiation (CSI), additional focal, or boost, radiation to the tumor bed and chemotherapy. As a result of radiation to the entire brain, patients commonly exhibit cognitive sequelae including fatigue and depression as well as decreases in intelligence quotient (IQ) and processing speed.[1,2]

The physical properties of proton therapy, including a sharp dose fall off at the Bragg peak, limits the amount of normal tissues exposed to radiation compared with standard photon therapy. For the CSI portion of treatment, anterior structures such as the heart and bowel are spared. It has been speculated that treatment with protons would reduce radiation-induced cognitive sequelae in medulloblastoma patients owing to sparing of normal brain tissues during the boost portion of treatment.[3] However, historically there has been a limited availability of proton therapy with a resulting paucity of clinical outcomes data.[4] Only recently have comparisons demonstrated a clinical benefit for cognitive sparing with protons compared with modern photon therapy.[5]

For both radiation types, the entire brain is treated to reduce recurrences. Thus, some degree of cognitive dysfunction is expected for both protons and photons. Although the reported superior outcomes in patients treated with protons, including stable global IQ, perceptual reasoning, and processing speed, may be due in part to normal tissue sparing during the boost portion of treatment, it is also possible that the relative biological effectiveness (RBE) of protons, as it relates to brain parenchyma damage and subsequent cognitive dysfunction, differs from the clinically used value of 1.1.[6]

This study aimed to compare and determine the differential effects of cranial irradiation when administered using both proton or photon irradiation in combination with advanced behavioral assays and imaging. To mimic clinical outcomes, including assessment of higher order cognitive domains beyond just memory, this study used a pediatric rat cranial irradiation model along with translational executive function cognitive testing including the 5-Choice Serial Reaction Time Task (5-CSRTT) to assess the longitudinal effect of radiation type, photon versus proton. Given reported differences in magnetic resonance imaging (MRI) changes being more prominent posttreatment in proton treated patients,[7-10] functional changes were evaluated using positron emission tomography (PET) and MRI, including connectomic metrics for comparison to cognitive testing outcomes. Connectome analysis is a useful imaging technique that can be used to investigate structural and functional changes of the neural network at the local and global level.[11] Imaging metrics derived from connectome analysis have also been found to be correlated to cognitive function and could therefore be a useful tool to noninvasively monitor radiation-induced changes after cranial radiation therapy (CRT).[12,13] Further characterization of molecular differences focused on brain inflammation which has a vital role in radiation-induced brain injury.[14]

Methods and Materials

Animals

Male Sprague Dawley rat pups (n = 12-15/group) were acquired with a mother (Envigo, Frederick, MD). At 10 to 12 days of age, animals were divided among 3 groups: sham, photon, and proton irradiation (see Figure E1 for an experimental timeline and for additional information). The Institutional Animal Care and Use Committees at Baylor College of Medicine and MD Anderson Cancer Center approved all animal experiments.

Irradiation

Animals were anesthetized before and during irradiation using an isoflurane/oxygen mixture. Animals were irradiated to the whole brain, excluding the olfactory bulb, at MD Anderson Proton Therapy Center. A Varian TrueBeam 6 MV beam with 2 lateral fields using a HD120 multileaf collimator was used for the photon cranial radiation therapy (X-CRT) to deliver a dose of 10 Gy to the whole brain. The whole brain proton cranial radiation therapy (P-CRT) consisted of a 100 MeV passively scattered beam spread-out Bragg peak using the Hitachi ProBeat delivery system. The

lateral proton beam had a range of 4.9 cm and spread-out Bragg peak of 3 cm delivering a biological dose of 10 Gy (RBE-weighted) over the entire brain assuming a constant RBE of 1.1 (Fig. E2).

Executive function

All animals were subjected to cognitive testing. As previously described, executive function was assessed using the 5-CSRTT (Med Associates, Fairfax, VT).[12,15] Before training and testing, animals were fasted to provide incentive for participation. Briefly, the testing equipment consists of a 5-chamber aperture which is illuminated individually during testing. The objective of the task is for the animal to nose-poke one of 5 apertures in which a stimulus light is shown. A food magazine dispenses a reward when the animal correctly pokes the illuminated aperture. Animals are first habituated to the apparatus and training consists of 35 daily sessions. During the training period, animals must meet specific set of criteria as established by Bari et al (accuracy, number of correct trials and omissions) at each stage before advancing to the next stage.[16] Animals have 30 minutes or 100 trials, whichever comes first, per day, to meet the set criteria. Stages increase in difficulty by shortening the stimulus duration, intertrial interval, and limited hold time. Training began at 3 months post-CRT. The final stage reached at the end of the training period is recorded as baseline. At 6- and 12-months post-CRT, animals were tested: 5 days at stage 7 (the average stage reached by the sham cohort during training period) and for an additional 5 days at stage 9 (as a way to challenge the animals). For each day of testing, animals have up to 30 minutes to complete 100 trials.

The following metrics were measured to determine each animal's cognitive performance: (1) percent accuracy (number of correct response over the total correct and incorrect responses); (2) percent correct (number of correct response over the total number of trials performed); (3) percent incorrect (number of incorrect response over the total number of trials performed); (4) premature responses (an attempt before the aperture is illuminated); and (5) perseverant responses (repeated attempt at illuminated aperture and number of omission: no response to stimulus). Theses metrics measure the animal's compulsive behavior, inhibitory response control, speed of information processing and decision making.[16] Analysis was performed for the first 3 days of testing to capture the learning and retention aptitude of the animal and before the task becomes repetitive.

Metabolic imaging

At 6 and 12 months post-CRT, animals (n = 8-9) were imaged with PET and computed tomography (CT) after receiving an injection of ^{18}F-Flurodeoxy-glucose (FDG). All PET/CT images were acquired on an Inveon scanner (Siemens AG, Knoxville, TN). Before imaging, animals were fasted for approximately 12 hours. One hour before scanning, each animal intravascularly received 12.58 MBq (340 μCi) of ^{18}F-FDG (Cyclotope). Animals were anesthetized with isoflurane gas and monitored during imaging to maintain normal breathing rates. CT scans were acquired first, followed by a 30-minute PET scan. The PET scans were reconstructed using OSEM3D and registered to the CT scan for attenuation correction. Using the acquired CT scan, regions were segmented using Inveon Research Workspace (Siemens AG). Uptake of radioisotope was measured using the standardized uptake value (SUV) and maximum SUV normalized to animal's body weight.

Magnetic resonance imaging

After completion of cognitive testing and in vivo imaging, animals (n = 7-9) were euthanized for ex vivo diffusion tensor imaging (DTI) using MRI scans. Samples were prepared according to the method described by Tyszka et al.[17] Brains were imaged using 20 distinct gradient directions on a 9.4T Bruker Biospec MRI scanner (Bruker BioSpin, Rheinstetten, Germany). All DTI reconstruction, tractography and connectome analyses were performed as described by Tang et al.[12] Briefly, connectomes were constructed for each animal with N = 132 nodes, network degree of E = number of edges, and a network density of $D = E/[(N \times (N\text{-}1))/2]$ representing the fraction of present connections to all possible connections.

The following connectome properties were calculated using graph theoretical analysis as implemented in the Brain Connectivity Toolbox to characterize global connectome effects: Trans = Transitivity; Assort = Assortativity; Eglob = Global Efficiency; Eloc = Local Efficiency; Mod = Modularity; λ = Characteristic Path Length; γ = Normalized Clustering Coefficient; and σ = Small Worldness Index (γ/λ).[18-20]

Using 100 null networks, λ is normalized by the mean path length and γ is normalized by mean clustering coefficient.[21] Data are presented as the area under curve across multiple densities or thresholds from minimum connection density to 60% connection. We measured regional connectome effects using the network-based statistic with 5000 permutations ($P < .05$, corrected).[22] We calculated mean length, volume, fractional anisotropy (FA) and apparent diffusion coefficient (ADC) for tractography virtual fibers. FA and ADC were calculated from the eigenvalues of the diffusion tensor as previously described.[23]

Immunohistochemistry

Whole brains (n = 4-5/group) were excised, fixed in 10% formalin, coronally sectioned, and embedded in paraffin. Fluorescent immunostaining was performed on 5μm sections after antigen retrieval in 95C sodium citrate buffer, followed by blocking in Sniper (Biocare Medical, Inc, Concord, MA). Primary antibodies were applied overnight for

myelin basic protein (MBP, 1:500, mouse, Abcam, Cambridge, UK), glial fibrillary acidic protein (1:400; goat, CST, Danvers, MA), and ionized calcium binding adaptor molecule 1 (1:400; goat, CST). Secondary antibodies (Invitrogen, Carlsbad, CA) conjugated to 488, 555, and 647 nm fluorophores (1/500, Alexafluor) appropriately matched to the primary antibody were incubated for 2 hours in the dark. Nuclei were visualized by DAPI (1/500). Two representative images per region were taken per section. Sections were imaged (20x, Nikon A1, Tokyo, Japan) at the dentate gyrus, cortex, and corpus callosum, and analyzed using ImageJ software (v.1.50i, NIH). All cells were counted manually per image per region and quantified relative to total proportion by DAPI presence. Myelin thickness was measured within the corpus callosum by MBP (1:500, mouse, Abcam) immunostaining with distance normalized to pixel size.

Statistical analysis

Statistical analyses were conducted using Prism 7 (GraphPad Software, Inc, La Jolla, CA). With multiple group comparison, a 1-way analysis of variance test was performed with Tukey correction with statistical significance was established at $P \leq .05$. Data are reported as mean ± standard error of the mean, unless otherwise noted. The first 3 days of testing were pooled for each animal. Connectome statistics were performed using permutation testing for global metrics and the network-based statistic for regional analysis.[22] Correlation analysis of imaging features and cognitive performance was performed using Pearson's correlation. P value for Pearson's correlation coefficient uses the t-distribution. Significance was established at $P \leq .05$.

Results

Radiation-induced phenotype

A radiation-induced phenotype was observed which consisted of irradiated animals having a smaller physique. This was observed at 3 months post-CRT, where both P-CRT ($P < .0001$) and X-CRT ($P < .0001$) were significantly lighter and shorter than sham animals. This phenotype persisted for the duration of the study. In addition, the proton irradiated group was significantly lighter than the photon irradiated group at 6 ($P = .018$) and 12 months post-CRT ($P = .046$) as well as significantly shorter in stature at 12 months post-CRT ($P = .0272$) (Fig. E3). Brain growth was also stunted, irradiated brains were lighter (P-CRT: $P = .02$, X-CRT: $P = .03$) and shorter (P-CRT: $P < .0001$, X-CRT: $P = .0015$) compared with sham animals with no significant differences between the 2 radiation modalities (Fig. E4).

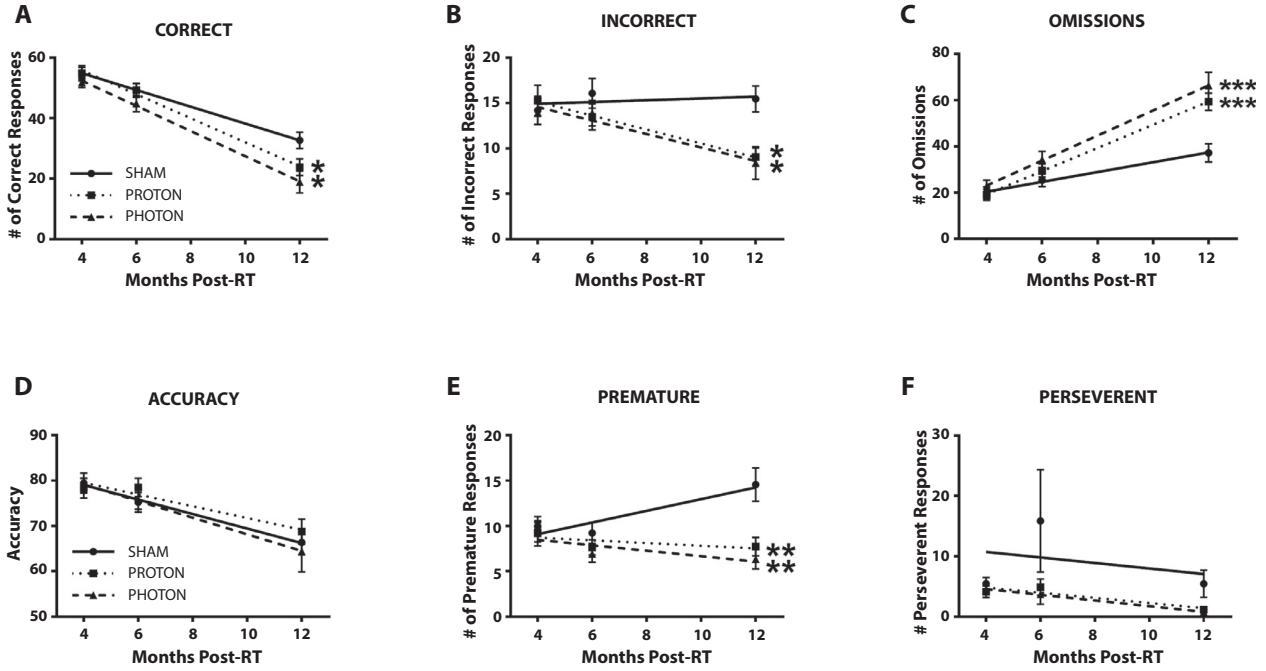

Fig. 1. The rate of change for the 5-choice serial reaction timed task testing metrics; (A) correct responses, (B) incorrect responses, (C) omissions, (D) accuracy, (E) premature responses, and (F) perseverant responses were assessed over time. All animals completed 100 trials per day of testing. Both photon and proton irradiated groups rates of decline were significantly steeper than sham for correct, incorrect, and premature responses. In addition, photon and proton irradiated groups had an increased rate of omissions overtime compared with the sham group. Mean ± standard error of the mean is shown, n = 15-12/group. *$P < .05$, **$P < .01$, and ***$P < .001$ compared with sham). *Abbreviation:* RT = radiation therapy.

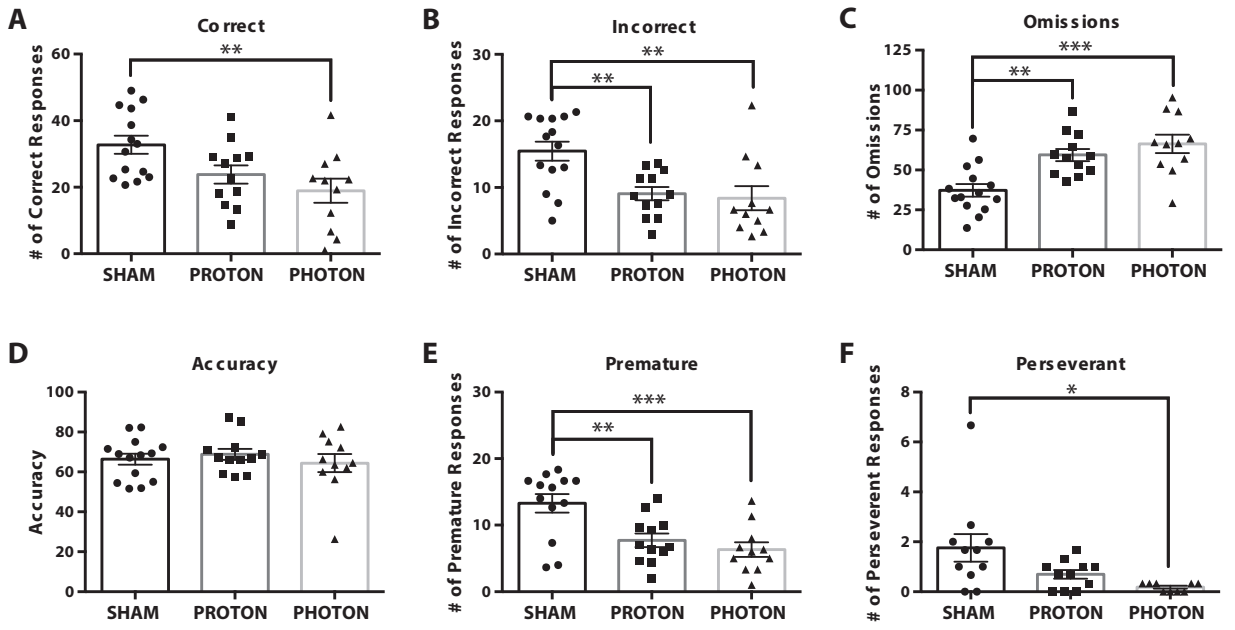

Fig. 2. Twelve months 5-choice serial reaction timed task testing results from stage 7. Several metrics were measured including (A) correct responses, (B) incorrect responses, (C) omissions, (D) accuracy, (E) premature responses, and (F) perseverant responses. Proton irradiated animals had significantly less incorrect and premature responses than sham but significantly more omissions. Photon irradiated animals had significantly less correct, incorrect, premature, and perseverant responses than sham and significantly more omissions. Mean ± standard error of the mean are shown, n = 15-12/group. *$P <$ .05, **$P <$ .01, and ***$P <$ .001

Cognitive rate of decline

Previous clinical studies have suggested a higher rate of cognitive decline in patients treated with photons compared with protons.[24] We therefore compared rates of cognitive deterioration over time between the irradiated and sham animals. The rate of cognitive deterioration over time for both P-CRT and X-CRT was significantly increased compared with sham for correct (P = .04 and P = .03, respectively), incorrect (P = .02 and P = .03, respectively), and omission (P = .0002 and P = .0003, respectively) responses (Fig. 1A-C). Unexpectedly, sham animals had a significant increase in the rate of premature responses overtime compared with P-CRT and X-CRT which maintained baseline levels (P = .01 and P = .004, respectively) (Fig. 1E). There was no significant change in the rate of decline for accuracy among the experimental groups (Fig. 1D). Also, there were no significant differences in slopes between P-CRT and X-CRT for any of the executive function parameters.

Executive function

During training at 3 months, on average, irradiated animals, P-CRT (6 ± 1.2 days) and X-CRT (6 ± 2 days), spent a longer amount of time in stage 5 than sham animals (5.1 ± 0.9 days) (Fig. E5A). However, the highest stage achieved among groups was not significantly different: sham (7.9 ± 0.4 stage achieved), P-CRT (8.0 ± 0.6 stage achieved), X-CRT (7.5 ± 0.5 stage achieved) (Fig. E5B). At 6 months, no significant differences were observed in executive function (Fig. E6). However, trends were observed demonstrating X-CRT animals having more cognitive dysfunction. At 12 months postradiation, regardless of irradiation type, there were significant changes in 5-CSRTT parameters associated with executive function, which includes attention and inhibitory control. There were significantly less incorrect and premature responses in both the P-CRT (9.1 ± 1.0, P = .0079; 7.7 ± 1.0, P = .0059) and X-CRT groups (8.4 ± 1.8, P = .0041; 6.3 ± 1.1 P = .0008) compared with the sham group (15.4 ± 1.4; 13.3 ± 1.4) (Fig. 2B,E). In addition, there were significantly more omissions in both the P-CRT (59 ± 4, P = .0029) and X-CRT (66 ± 6, P = .0002) groups compared with the sham group (37 ± 4) (Fig. 2C). However, only the X-CRT group had significantly less correct (19 ± 4, P = .0072) and perseverant responses (0.18 ± 0.06, P = .0134) than sham animals (33 ± 3; 1.8 ± 0.6, respectively) (Fig. 2A,F). There were no significant differences found between P-CRT and X-CRT for any 5-CSRTT metric.

Tractography virtual fiber measurements

The parameters calculated from diffusion MRI tractography data showed mixed results. FA was not found to be different between sham and the 2 irradiated groups for whole brain. Segmentation of 66 different brain regions found no

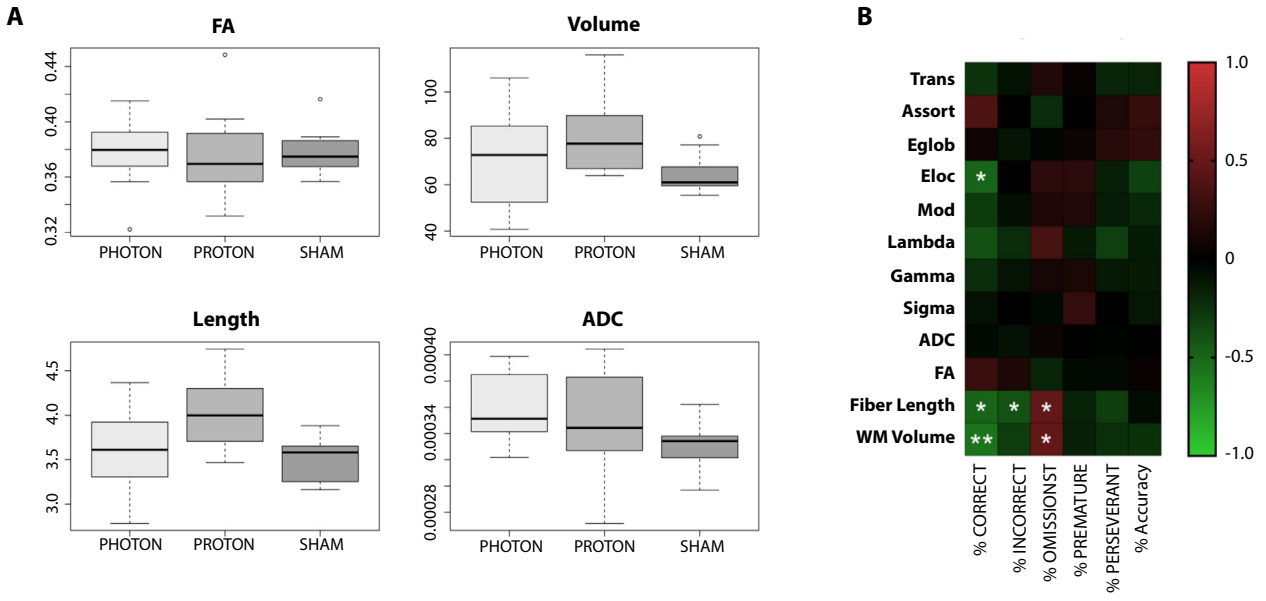

Fig. 3. Parameters calculated from diffusion magnetic resonance imaging data are informative of cognitive performance. (A) Although fractional anisotropy (FA) was not different between sham and the 2 irradiated groups, white matter volume and fiber length, only in the proton group, both showed significantly higher values compared with sham ($P = .03$). The photon group has the highest apparent diffusion coefficient (ADC) which is significantly different from sham ($P = .04$) but not proton ($P = .61$; proton vs. sham $P = .370$. Data are shown as box-and-whisker plot: box extends from the 25th to 75th percentiles, median value marked by line and whiskers extend from min to max, n = 7-9/group. (B) Correlation of the connectomic metrics and 5-choice serial reaction time task testing at 12 months postirradiation. *$P < .05$ and **$P < .01$.

significant difference between the groups (Table E1). Both white matter volume and fiber length showed significantly higher values compared with sham ($P = .03$), but only in the *P*-CRT group. The X-CRT group had the highest ADC which was significantly different from sham ($P = .04$), but P-CRT ADC was not different from sham (Fig. 3A).

Connectome

Late term connectomic changes were assessed in irradiated brains. Regardless of irradiation type, there were no significant differences in global connectomic measures (Fig. E7). The results from regional connections show that P-CRT brains demonstrated significant hypo-connectivity of 43 connections compared with sham animals, whereas X-CRT brains only had one altered connection compared with sham (Table E2).

Correlation

To identify an imaging signature of cognitive changes, correlative analysis was carried out between the 5-CSRTT and connectomic parameters at 12 months. Significant negative correlations were found between 5-CSRTT Percent Correct and Local efficiency, fiber length, and white matter volume. Correlation was also found between Percent Incorrect and fiber length. In addition, Percent Omission was found to be significantly correlated with both fiber length and white matter volume (Fig. 3B).

Brain glucose metabolism

Brain glucose metabolism was assessed using ^{18}F-FDG PET imaging. At 6 months postirradiation, regardless of type of irradiation, no significant increase in glucose consumption was measured in the brain (Fig. 4). However, at 12 months postirradiation, X-CRT showed a significant increase (4.9 ± 0.2 SUV, $P = .0428$) in brain glucose metabolism compared with sham (2.7 ± 0.7 SUV). Brain glucose consumption in the P-CRT animals at 12 months postirradiation was not significantly different from the sham group.

Immunohistochemistry

Immunostaining at 12 months post-CRT indicates late-term inflammation shown by proportionally higher enhanced microglial and astroglial presence as well as myelin thinning in irradiated brains. Global inflammation was observed in both X-CRT and P-CRT brains within the dentate gyrus (P-CRT: $P = .004$, X-CRT: $P = .0004$), corpus callosum (P-CRT: $P = .008$, X-CRT: $P = .0007$), and cortex (P-CRT: $P = .004$, X-CRT: $P = .0004$) having significantly higher number of astrocytes (glial fibrillary acidic protein) compared with sham (Fig. 5). X-CRT brain had higher number of

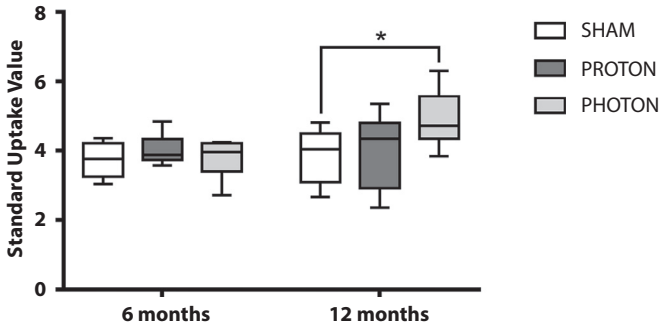

Fig. 4. Brain glucose metabolism was significantly higher in the photon irradiated group measured using ^{18}F-Flurodeoxyglucose using positron emission tomography imaging at 6 and 12 months postirradiation. Data are shown as box-and-whisker plot: box extends from the 25th to 75th percentiles, median value marked by line and whiskers extend from min to max, n = 8-9/group (*$P < .05$).

astrocytes in all the regions analyzed compared with P-CRT. Irradiated brains also had significantly higher number of activated microglia (ionized calcium binding adaptor molecule 1) in the dentate gyrus (P-CRT: $P = .03$, X-CRT: $P = .006$) compared with sham animals (Fig. 5). These results indicate that there are late-term low levels of inflammation. Although not significantly different, X-CRT showed a trend toward having higher inflammatory effect. In addition, analysis of the

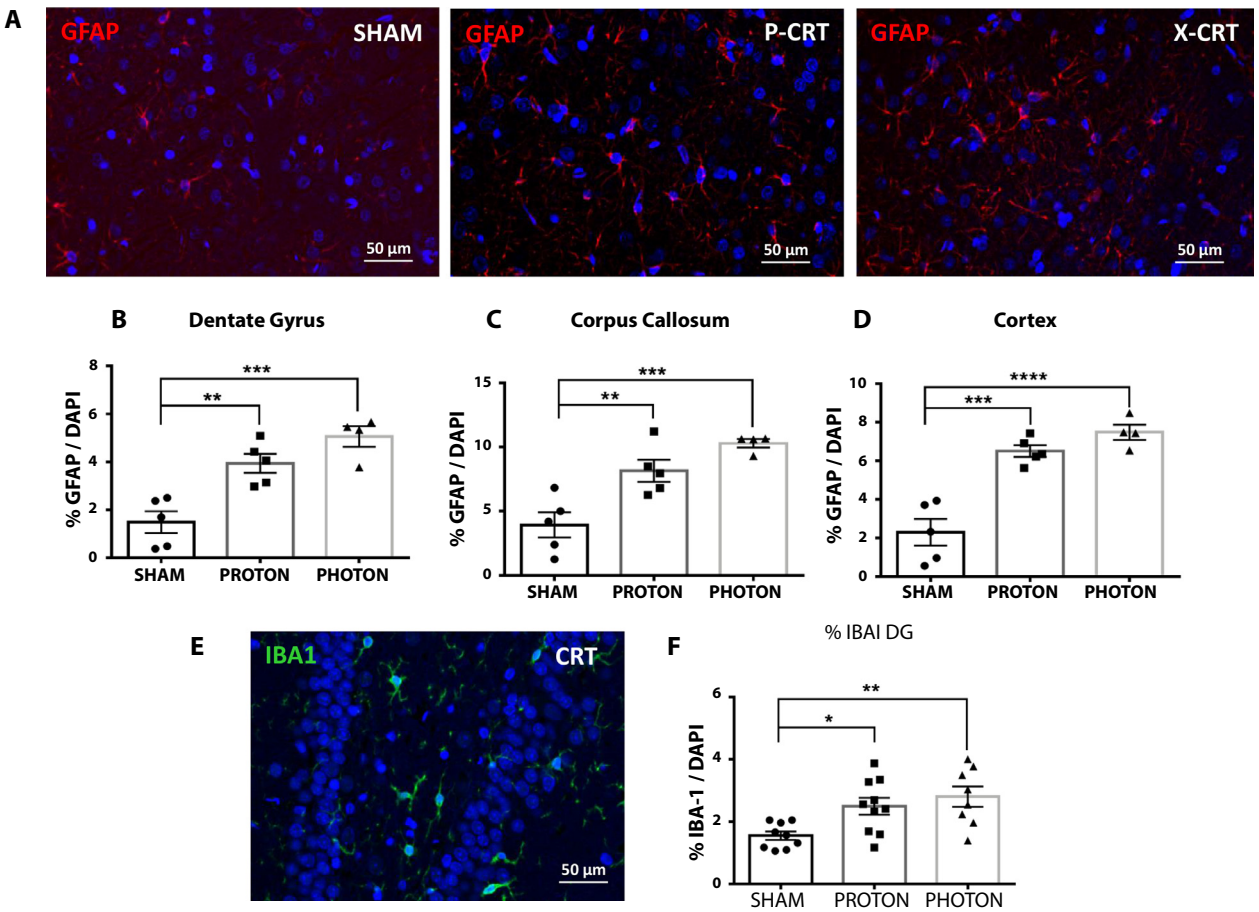

Fig. 5. Neuroinflammation was observed throughout the brain at 12 months post-CRT. (A) Brain sections immunostained for glial fibrillary acidic protein (GFAP) in sham, P-CRT, and X-CRT cortexes. An increase in GFAP positive cells was observed throughout the brain in the (B) dentate gyrus, (C) corpus callosum, and (D) cortex. (E) Brain section stained for activated microglia in the dentate gryus. (F) Quantification of ionized calcium binding adaptor molecule 1 (IBA-1)−positive cells in the dentate gyrus. Counting was done in duplicate. Mean ± standard error of the mean are shown, n = 4-5 animals/group. *$P < .05$, **$P < .01$, ***$P < .001$, and ***$P < .0001$. Scale bar represents 50 μm. *Abbreviations*: CRT = cranial radiation therapy; P-CRT = proton cranial radiation therapy; X-CRT = photon cranial radiation therapy.

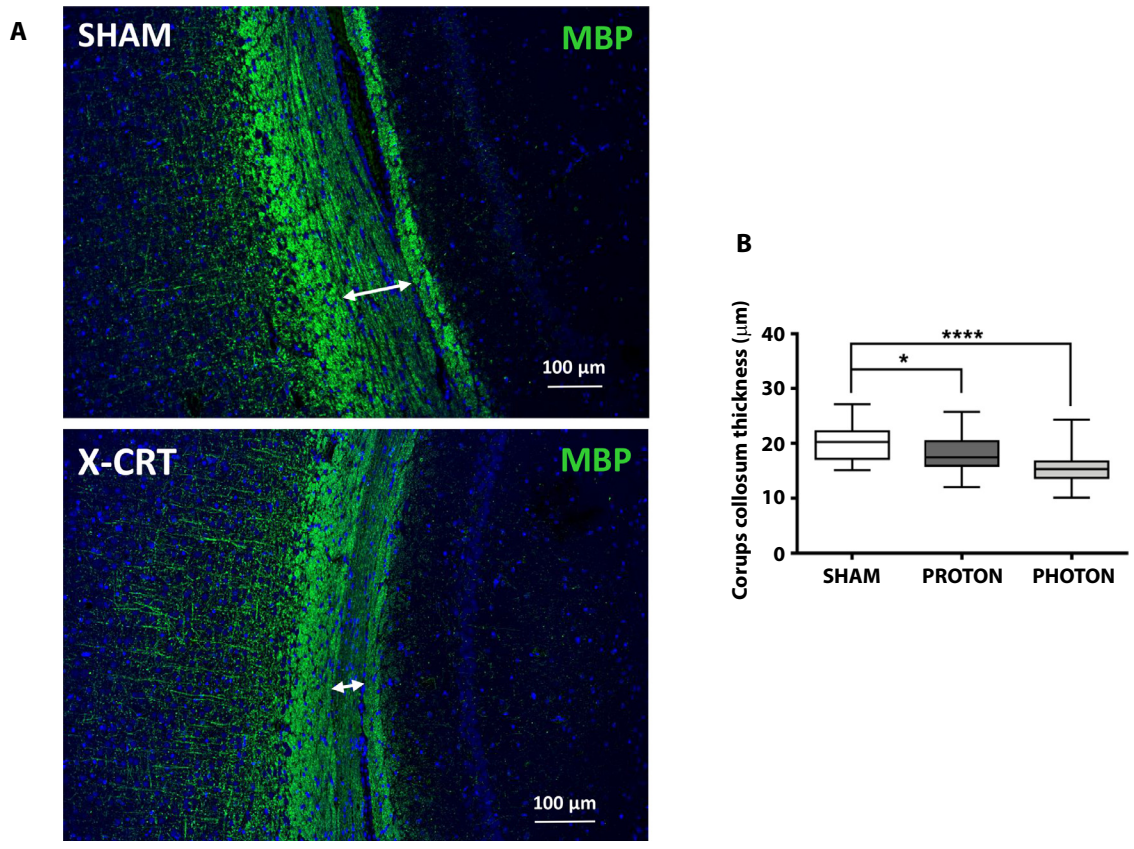

Fig. 6. CRT brain at 12 months post-CRT showed significant myelin thinning. (A) CRT brain sections immunostained for myelin basic protein (MBP) in sham (top) vs X-CRT (lower), and (B) quantification of the corpus callosum thickness. Data are shown as box-and-whisker plot: box extends from the 25th to 75th percentiles, median value marked by line and whiskers extend from min to max, n = 4-5/group. *$P < .05$ and ****$P < .0001$. Scale bar represents 100 μm. *Abbreviations*: CRT = cranial radiation therapy; X-CRT = photon cranial radiation therapy.

corpus callosum showed a significant reduction in myelin thickness (P-CRT: $P = .017$, X-CRT: $P < .0001$) in irradiated animals with X-CRT animals having a more significant reduction (Fig. 6).

Discussion

Clinical data are emerging to suggest that proton therapy may offer superior cognitive sparing compared with standard photon-based therapies.[24] Therefore, it is important to compare the biological effectiveness of the 2 radiation types as it relates to normal brain damage. Although no major differences might be expected, to our knowledge no preclinical studies have addressed this. Here we compared the effects of whole brain radiation delivered with clinically representative proton or photon beams and found similar effects. We observed significant differences in cognitive measurements for the number of correct and perseverant responses between X-CRT and sham that were not observed in the P-CRT group. We also measured differences in imaging response for both PET and MRI between the radiation types which warrants further study. This study also identified connectome and white matter–based imaging features that are indicative of executive performance. Lastly, late-term immunoflurescence differences were observed which demonstrated signs of both radiation-induced neuroinflammation and demyelination but were not significantly different between the radiation modalities. Nevertheless, X-CRT trended toward being consistently more damaging than *P*-CRT.

Executive function, mediated by the frontal lobe, describes the cognitive process of the brain involved in working memory, inhibitory control, attention, mental flexibility, and planning and organizing. Survivors of medulloblastomas commonly have impairment associated with executive function.[1] As a result, this work used the 5-CSRTT to measure the effect of both proton and photon CRT on executive function in rodents. Similar to the findings by Sahnoune et al[15] and Tang et al,[12] which also used 5-CSRTT to measure executive function, we also measured an overall radiation effect on executive function. Irradiated animals had significantly higher number of omissions, which is scored when no attempt is made during the duration of the stimulus. We speculate that this is indicative of deficit in attention which has been observed in pediatric

patients with localized brain tumors treated with radiation therapy.[25] Irradiated animals were found to have similar activity levels as sham animals based on their time to response in 5-CSRTT (data not shown) and did not display any depressive behavior that could contribute to the higher number of omissions. The observed higher number of omissions with no significant difference in accuracy seems to indicate that irradiated animals are still able to perform this higher order cognitive test but lack the attention and focus. We measured significantly more metrics associated with cognitive decline in the X-CRT animals than in the P-CRT animals; however, when photon and proton groups were compared there was no significant difference found between them. These findings recapitulate clinical findings presented by Kahalley et al,[24] in which photon treated patients had significantly greater declines in IQ but there was no significant difference between proton- and photon-treated patients compared together. Antonini et al[26] has also seen limited changes in executive function in proton cranial spinal irradiated patients compared with normal, noting that the comparison was to focal proton irradiation and not to photon CSI.

Even though significant differences were observed in cognition between irradiated animals and sham, the groups did not differ significantly in connectome organization. Because of the high dimensionality of connectome data, larger samples may be required. Alternate connectome approaches such as multimodal imaging and/or different parcellation methods might yield different results. However, the 2 irradiated groups did show unique profiles of connectome organization compared with sham animals and connectome metrics were correlated with certain cognitive measures. At the same time, there were significant differences in white matter volume and fiber length between sham and proton animals. Although significant myelin thinning was found in the corpus callosum between irradiated animals and sham, there was no significant difference in FA between the groups. The discrepancy between the imaging metric and immunofluorescence results could be due to the sensitivity of our imaging technique.

In addition to connectome analysis, which provide functional and structural metrics of the local and global network, other diffusion based imaging techniques have also been used to characterize radiation-induced brain injury.[27-29] In a study by Constanzo et al, diffusion MRI metrics, including FA, mean diffusivity, axial diffusivity, and radial diffusivity, were found to be significantly different after localized irradiation.[27] Results from our study however did not find FA changes in any of the brain regions. This may be owing to differences between the radiation dose used, and our study used a lower radiation dose and younger animals compared with the other study. This highlights the need for further validation of the sensitivity of these imaging techniques to radiation dose before these imaging metrics can be used in the clinic.

Imaging metrics may also be informative of cognitive function. White matter volume was found to be negatively correlated with percent correct and positively correlated with percent omission which seems to indicate that reduction of white matter volume is associated with better cognitive function. This finding however is inconsistent with clinical data where white matter volume reduction was associated with decreased cognitive performance in medulloblastoma patients treated with CRT.[30] The discrepancy could be due to the difference in the relative white matter volume in humans and rodent models.[31] In terms of connectome features, local efficiency and percent correct seems to indicate that local specialization, and, therefore, network segregation is associated with decreased cognitive impairment. In their CRT model, Sahnoune et al also found local damage to network connectivity with CRT animals having lower global efficiency.[15] Further studies are needed to validate these imaging features, but they could be used as a tool to monitor cognitive changes without extensive behavioral testing.

Brain glucose consumption is primarily via neurons but is regulated by astrocytes.[32] In rats, an increase in brain glucose consumption corresponded with brain areas of increased activation as measured using MR blood oxygen level detection imaging.[33] In the current study, we measured a global increase in brain glucose metabolism in the X-CRT but not in P-CRT animals. This is similar to previous results where we have seen an increase in brain glucose metabolism at 12 months post-CRT, albeit at a much higher radiation dose of 30 Gy.[12] Similar late-term imaging findings have also been measured by Krull et al in acute lymphoblastic leukemia patients who had received cranial irradiation but who were also treated with chemotherapy.[34] We and others have shown that the increase in brain glucose consumption coincides with an increase in brain inflammation.[12,35] These findings are in agreement with the ADC data presented in Figure 3 which show a greater change in the X-CRT group's apparent diffusion compared with the P-CRT group. Immunohistochemistry further confirms these imaging results, however statistical significance was not established between P-CRT and X-CRT. We did show that X-CRT trended toward having more astrocytes and activated microglia. Although analysis of the corpus callosum found significant myelin thinning, imaging results indicated total white matter volume and average global fiber length were higher in both groups compared with sham but significance was only established in the P-CRT and not X-CRT group. This seems to indicate that loss of white matter is not homogenous. Again, we observed trends toward more damage in the X-CRT group with more myelin thinning, less white matter volume, and reduced average fiber length.

Study limitations

There are several limitations to the present study. We irradiated the whole brain of the animals to mirror clinical CSI treatments, but this setup does not account for

the decreased entrance and exit dose of P-CRT compared with X-CRT. Although this radiation scheme does not recapitulate the boost portion of the CSI treatment plan, it allows for the direct comparison of photon and proton irradiation, RBE-weighted dose, in the normal brain tissue. The study was limited to male pediatric (10-12 days of age) rats which approximately corresponds to a 3-year-old child, the earliest in which CRT would be used to treat brain tumors.[36] The findings may differ if animals were irradiated at a different age, but younger animals display increased sensitivity to radiation effects, which should increase the power of our assays to discern differences between the 2 radiation modalities. In addition, this study was designed as a single-dose comparison assuming a proton RBE of 1.1. Therefore, conclusions from this study are limited to this single RBE value. The inability to detect a difference between P-CRT and X-CRT may also be due to the study's sample size, but it may also be that the RBE for normal tissue toxicity is 1. This study is limited to the 5-CSRTT, a frontal lobe executive function task; however, the inclusion of other cognitive tests could reveal deficits in other cognitive domains. We chose to test the same group of animals over time, which could be considered enrichment and may have minimized the measured radiation induced changes in imaging and cognition at later time points. Furthermore, owing to a lengthy DTI scan time, ~18 hours, DTI was only performed at 12 months in ex vivo brains.

Conclusions

Overall, we found evidence that CRT negatively affects executive function with long-term imaging changes. Compared with sham animals, there were subtle differences between P-CRT and X-CRT animals. However, there were no significant differences between the 2 types of irradiation when compared against each other. There were imaging differences found in glucose metabolism, white matter volume, fiber length, and brain ADC values between both P-CRT and X-CRT and sham animals but not against one another. Although statistical significance could not be established with the cognitive, imaging, and immunofluorescent measurements, there were trends toward X-CRT animals having more impairment and inflammation in brain cells. Although the results do not reject the assumption of an RBE of 1.1, they indicate that not all differential effects are encapsulated with the assumed RBE of 1.1 in normal brain tissue and thus warrant further investigation. This study also identified imaging markers reflective of cognitive changes and that therefore could provide clinicians with an additional tool to monitor patients and as a tool to noninvasively evaluate the efficacy of different interventions. Further studies need to be conducted to elucidate the underlying biology responsible for the imaging differences found.

References

1. Brinkman TM, Reddick WE, Luxton J, et al. Cerebral white matter integrity and executive function in adult survivors of childhood medulloblastoma. *Neuro Oncol* 2012;14 Suppl 4(Suppl 4):iv25–iv36.
2. Palmer SL, Armstrong C, Onar-Thomas A, et al. Processing speed, attention, and working memory after treatment for medulloblastoma: An international, prospective, and longitudinal study. *J Clin Oncol* 2013;31:3494–3500.
3. Ho ESQ, Barrett SA, Mullaney LM. A review of dosimetric and toxicity modeling of proton versus photon craniospinal irradiation for pediatrics medulloblastoma. *Acta Oncol* 2017;56:1031–1042.
4. Ramaswamy V, Remke M, Bouffet E, et al. Risk stratification of childhood medulloblastoma in the molecular era: The current consensus. *Acta Neuropathol* 2016;131:821–831.
5. Kahalley LS, Peterson R, Ris MD. Superior intellectual outcomes after proton radiotherapy compared with photon radiotherapy for pediatric medulloblastoma. *J Clin Oncol* 2020;38:454–461.
6. Paganetti H, Niemierko A, Ancukiewicz M, et al. Relative biological effectiveness (RBE) values for proton beam therapy. *Int J Radiat Oncol Biol Phys* 2002;53:407–421.
7. Gunther JR, Sato M, Chintagumpala M, et al. Imaging changes in pediatric intracranial ependymoma patients treated with proton beam radiation therapy compared to intensity modulated radiation therapy. *Int J Radiat Oncol Biol Phys* 2015;93:54–63.
8. Ludmir EB, Mahajan A, Paulino AC, et al. Increased risk of pseudoprogression among pediatric low-grade glioma patients treated with proton versus photon radiotherapy. *Neuro Oncol* 2019;21:686–695.
9. McGovern SL, Okcu MF, Munsell MF, et al. Outcomes and acute toxicities of proton therapy for pediatric atypical teratoid/rhabdoid tumor of the central nervous system. *Int J Radiat Oncol Biol Phys* 2014;90:1143–1152.
10. Bronk JK, Guha-Thakurta N, Allen PK, Mahajan A, Grosshans DR, McGovern SL. Analysis of pseudoprogression after proton or photon therapy of 99 patients with low grade and anaplastic glioma. *Clin Transl Radiat Oncol* 2018;9:30–34.
11. Sporns O. The human connectome: a complex network. *Ann N Y Acad Sci* 2011;1224:109–125.
12. Tang TT, Zawaski JA, Kesler SR, et al. A comprehensive preclinical assessment of late-term imaging markers of radiation-induced brain injury. *Neurooncol Adv* 2019;1:vdz012.
13. Kesler SR, Petersen ML, Rao V, Harrison RA, Palesh O. Functional connectome biotypes of chemotherapy-related cognitive impairment. *J Cancer Surviv* 2020;14:483–493.
14. Beamish CA, Zawaski JA, Inoue T, et al. NF-κB blockade by NEMO binding domain peptide ameliorates inflammation and neurobehavioral sequelae after cranial radiation therapy in juvenile mice. *Int J Radiat Oncol Biol Phys* 2021;109:1508–1520.
15. Sahnoune I, Inoue T, Kesler SR, et al. Exercise ameliorates neurocognitive impairments in a translational model of pediatric radiotherapy. *Neuro Oncol* 2018;20:695–704.
16. Bari A, Dalley JW, Robbins TW. The application of the 5-choice serial reaction time task for the assessment of visual attentional processes and impulse control in rats. *Nat Protoc* 2008;3:759–767.
17. Tyszka JM, Readhead C, Bearer EL, Pautler RG, Jacobs RE. Statistical diffusion tensor histology reveals regional dysmyelination effects in the shiverer mouse mutant. *Neuroimage* 2006;29:1058–1065.
18. Rubinov M, Sporns O. Complex network measures of brain connectivity: uses and interpretations. Neuroimage 2010;52:1059–1069.
19. Sporns O, Betzel RF. Modular brain networks. *Annu Rev Psychol* 2016;67:613–640.
20. Bassett DS, Bullmore E. Small-world brain networks. Neuroscientist 2006;12:512–523.
21. Zalesky A, Fornito A, Bullmore E. On the use of correlation as a measure of network connectivity. *Neuroimage* 2012;60:2096–2106.
22. Zalesky A, Fornito A, Bullmore ET. Network-based statistic: identifying differences in brain networks. *Neuroimage* 2010;53:1197–1207.

23. Soares JM, Marques P, Alves V, Sousa N. A hitchhiker's guide to diffusion tensor imaging. *Front Neurosci* 2013;7:31.
24. Kahalley LS, Ris MD, Grosshans DR, et al. Comparing intelligence quotient change after treatment with proton versus photon radiation therapy for pediatric brain tumors. *J Clin Oncol* 2016;34:1043–1049.
25. Merchant TE, Kiehna EN, Miles MA, Zhu J, Xiong X, Mulhern RK. Acute effects of irradiation on cognition: Changes in attention on a computerized continuous performance test during radiotherapy in pediatric patients with localized primary brain tumors. *Int J Radiat Oncol Biol Phys* 2002;53:1271–1278.
26. Antonini TN, Ris MD, Grosshans DR, et al. Attention, processing speed, and executive functioning in pediatric brain tumor survivors treated with proton beam radiation therapy. *Radiother Oncol* 2017;124:89–97.
27. Constanzo J, Dumont M, Lebel R, et al. Diffusion MRI monitoring of specific structures in the irradiated rat brain. *Magn Reson Med* 2018;80:1614–1625.
28. Perez-Torres CJ, Engelbach JA, Cates J, et al. Toward distinguishing recurrent tumor from radiation necrosis: DWI and MTC in a Gamma Knife−irradiated mouse glioma model. *Int J Radiat Oncol Biol Phys* 2014;90:446–453.
29. Rodgers SP, Zawaski JA, Sahnoune I, Leasure JL, Gaber MW. Radiation-induced growth retardation and microstructural and metabolite abnormalities in the hippocampus. *Neural Plast* 2016;2016:3259621.
30. Reddick WE, Glass JO, Palmer SL, et al. Atypical white matter volume development in children following craniospinal irradiation. *Neuro Oncol* 2005;7:12–19.
31. Ventura-Antunes L, Mota B. Herculano-Houzel S. Different scaling of white matter volume, cortical connectivity, and gyrification across rodent and primate brains. *Front Neuroanat* 2013;7:3.
32. Magistretti PJ. Neuron-glia metabolic coupling and plasticity. *Exp Physiol* 2011;96:407–410.
33. Wehrl HF, Hossain M, Lankes K, et al. Simultaneous PET-MRI reveals brain function in activated and resting state on metabolic, hemodynamic and multiple temporal scales. *Nat Med* 2013;19:1184–1189.
34. Krull KR, Minoshima S, Edelmann M, et al. Regional brain glucose metabolism and neurocognitive function in adult survivors of childhood cancer treated with cranial radiation. *J Nucl Med* 2014;55:1805–1810.
35. Brabazon F, Wilson CM, Shukla DK, et al. [18F]FDG-PET Combined with MRI elucidates the pathophysiology of traumatic brain injury in rats. *J Neurotrauma* 2017;34:1074–1085.
36. Sengupta P. The laboratory rat: Relating its age with human's. *Int J Prev Med* 2013;4:624–630.